The Ring Vortex: Concepts for a Novel Complex Flow Phantom for Medical Imaging

Simone Ferrari[1,2]*, Simone Ambrogio[1,2,3]*, Adrian Walker[3], Prashant Verma[4], Andrew J. Narracott[1,2], Iain Wilkinson[5], John W. Fenner[1,2]

[1]Medical Physics, Mathematical Modelling in Medicine Group, Department of Infection, Immunity and Cardiovascular Disease, University of Sheffield, Sheffield, UK
[2]Insigneo Institute for In Silico Medicine, University of Sheffield, Sheffield, UK
[3]Leeds Test Objects Ltd., Boroughbridge, UK
[4]Medical Imaging & Medical Physics, Sheffield Teaching Hospitals NHS Foundation Trust, Sheffield, UK
[5]Academic Unit of Radiology, Department of Infection, Immunity and Cardiovascular Disease, University of Sheffield, Sheffield, UK
Email: sferrari1@sheffield.ac.uk

Abstract

Calibration of medical imaging systems that provide quantitative measures relating to complex physiological flows is challenging. Physical test objects available for the purpose either offer a known simple flow far removed from the complexity of pathology (e.g. parabolic flow in a straight pipe) or complex relevant flows in which the details of the flow behaviour are unknown. This paper presents the ring vortex as a candidate for a complex flow phantom, since it is marked by inherently complex flow features that are controllable, predictable, reproducible and stable. These characteristics are demonstrated by a combination of analytical, numerical (CFD) and experimental methods. Together they provide a consistent perspective on ring vortex behaviour and highlight qualities relevant to phantom design. Discussion of the results indicates that a liquid phantom based on the ring vortex may have merit as a complex flow phantom for multimodal imaging. Furthermore, availability of such a flow reference may also serve as a benchmark for quality assurance of simulation methodologies.

Keywords

Imaging, Phantom, Flow, Vortex

1. Introduction

This paper argues for a novel concept in medical imaging flow phantom design based around the flow phenomenon known as the ring vortex. Relevant medical

---

*The first two authors contributed equally to the preparation of this manuscript.

imaging technologies include Doppler ultrasound, and (contrast) angiography techniques that involve planar X-ray, MRI and CT [1] [2] [3] [4]. Analysis of physiological flows plays a fundamental role in diagnosis of numerous pathologies and for this reason it is important that flow-informed diagnosis is both sensitive and specific, based on flow-derived metrics that can reliably support clinical decision making [5] [6]. Flow phantoms provide a mechanism by which diagnostic performance of the imaging technology can be calibrated and evaluated. In the context of numerical simulation, patient-specific analysis is often informed using both the geometry and the flow information obtained from imaging studies. Flow phantoms also offer a means by which high quality numerical and experimental benchmark data can be provided to undertake Quality Assurance of simulation methodologies, as exemplified by the recent FDA critical path initiative [7]. A well specified phantom can give confidence to interpretation of flow data.

Flow related quantities obtained from imaging systems vary according to scanner technology and performance. Assessment of the latter is recommended through approved quality assurance and control processes[1] [8] [9] that aim to uncover nonconformity and identify deviations from product performance specification [10]. Evaluation of performance is typically made through the acquisition of images obtained using a test object specifically designed to provide consistent results. If the measured parameters differ greatly from reference values (exceeding defined tolerances), then interpretation is compromised and may discourage the imaging system from being used. Medical imaging phantoms are constructed according to precise specifications that ensure consistent measurements for medical device evaluation/calibration. Ideally a flow phantom should produce a known flow field and mimic the *in vivo* situation, including motion. This is challenging, and in reality physical flow phantoms deliver either (i) a complex flow (whose precise details are unknown) based on a rig whose flows are physiologically relevant [11] [12], or (ii) a simple flow (or alternative [10]) that is explicitly known, designed specifically for scanner calibration/assessment [13] [14] [15]. Arguably many current phantom designs implement flows that bear little resemblance to the complex physiological and pathological flows encountered in the clinic (*i.e.* basic steady flows and/or pulsatile simple flows are commonly implemented), and those that attempt greater complexity must accept many ambiguities in the flow environment. Such issues also have wider ramifications, since patient-specific computational fluid dynamics (CFD) may be used to infer complex flows from image-derived geometries. However, the lack of a gold standard reference in such conditions often limits the degree to which inferred flow measures can be trusted, regardless of whether the flow is derived from computational or image-based approaches.

We propose a new reference for complex flow imaging in the form of the ring

---

[1]Quality Control (QC) refers to "part of quality management focused on fulfilling quality requirements"—ISO 9000 clause 3.2.10.

Quality Assurance (QA) refers to "a part of quality management focused on providing confidence that quality requirements will be fulfilled"—ISO 9000 clause 3.2.11.

vortex. This benchmark flow can be studied as a physical phantom for imaging performance assessment, and may also be useful as a reference for quality assurance of computational approaches. It offers the capacity to produce known complex flow features (velocity, acceleration, pulsatility, vorticity, etc.) that are predictable, reproducible, controllable and stable. Consequently, practical experience of the ring vortex is described below and its suitability as a candidate for an innovative complex flow phantom is discussed and presented.

1.1. What Is the Ring Vortex?

The ring vortex is a fundamental component of flow complexity and consists of an annular vortex core that propagates perpendicular to the plane of the ring. It is a natural phenomenon that is variously known as a "ring vortex", "smoke ring" or "toroidal vortex". Ring vortices represent one of the most fundamental phenomena in fluid dynamics. As described by Akhmetov "…a vortex ring is a toroidal volume of vortical fluid moving in a surrounding medium at an approximately constant translational speed perpendicular to the ring plane. The fluid motion is axisymmetric, and the vector of vorticity in the torus is directed along the circles concentric with the circular axis of the torus. A certain volume of the fluid which embraces the ring and looks like an ellipsoid flattened along the direction of motion is moving together with the toroidal vortex ring. This enclosed volume of fluid is called vortex atmosphere. Inside the vortex atmosphere the fluid is circulating along the closed streamlines encompassing the toroidal core of the vortex. Motion of the fluid surrounding the vortex atmosphere resembles a pattern of flow without separation past a corresponding solid body." [16] (see the schematic stream functions of **Table 1**).
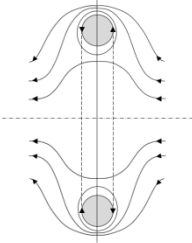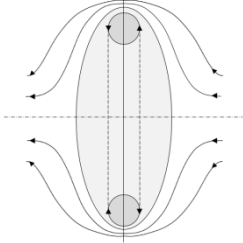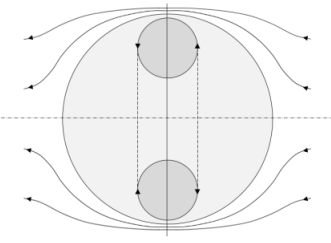
The vortex ring clearly offers vorticity, but because it is stable and can be controlled it also offers reproducibility, pulsatility, and can be produced in various sizes, travelling at distinct velocities. These characteristics make it particularly suitable as a candidate for a complex flow phantom. As an illustration of its predictability, reproducibility, controllability and stability, the following sections present analytical and computational analyses of the ring vortex, as well as our own experimental experiences with this phenomenon. Together they provide a body of evidence, considered in the discussion section, which is used to evaluate the suitability of this flow for calibration and performance evaluation of medical imaging systems and benchmarking of computational simulations.

2. Methods

2.1. Analytical

The behaviour of the ring vortex can be generally described by solution of the Navier-Stokes equations [17]. An incompressibility assumption simplifies the description, but only under highly idealised and axisymmetric conditions is the behaviour amenable to analytical solution [18]. The preferred description is in terms of the stream function Ψ. It is natural to consider the ring vortex moving at velocity v within a static free field, but the stream function solution changes

Table 1. Analytical descriptions of ring vortex properties consistent with the Navier-Stokes equations.

Model (class)	Thin (Lamb) [22]	Thick (Kaplanski-Rudi) [21]	Spherical (Hill) [18]
Schematic Stream Function Ψ			
Circulation Γ	Const Γ	$\Gamma = \dfrac{I}{\pi R^2}\left[1 - \exp\left(-\dfrac{\tau^2}{2}\right)\right]$	$\Gamma = 5av$
Impulse I	$I = \rho\Gamma\pi R^2$	Const I	$I = 2\rho\pi a^3 v$
Energy E	$E = \dfrac{1}{2}\rho\Gamma^2 R\left[\ln\dfrac{8R}{a} - \dfrac{7}{4}\right]$	$E = \dfrac{I^2}{2\pi^2}\dfrac{\tau}{R^3}\left[\dfrac{1}{12}\sqrt{\pi}\tau^2\,_2F_2\left(\left\{\dfrac{3}{2},\dfrac{3}{2}\right\},\left\{\dfrac{5}{2},3\right\},-\tau^2\right)\right]$	$E = \left(\dfrac{10}{7}\right)\rho\pi a^3 v^2$
Velocity v	$v = \dfrac{\Gamma}{4\pi R}\left(\ln\dfrac{8R}{a} - \dfrac{1}{4}\right)$	$v = \dfrac{I}{4\pi^2}\dfrac{\tau}{R^3}\left\{3\sqrt{\pi}\exp\left(-\dfrac{\tau^2}{2}\right)I_1\left(\dfrac{\tau^2}{2}\right)\right.$ $+ \dfrac{1}{12}\sqrt{\pi}\tau^2\,_2F_2\left(\left\{\dfrac{3}{2},\dfrac{3}{2}\right\},\left\{\dfrac{5}{2},3\right\},-\tau^2\right)$ $\left. - \dfrac{3}{5}\sqrt{\pi}\tau^2\,_2F_2\left(\left\{\dfrac{3}{2},\dfrac{5}{2}\right\},\left\{2,\dfrac{7}{2}\right\},-\tau^2\right)\right\}$	Const v

Symbols: ρ is the fluid density; R is the ring radius; a is the core radius (see **Figure 1**); $\tau = R/l$ where l is the diffusivity scale of the ring's core; I_1 is the first-order modified Bessel function; $_2F_2$ is the generalized hypergeometric function.

the frame of reference so that the ring is static as the free field passes at velocity -v. Broadly speaking the analytical solutions can be characterised according to three particular idealizations, namely:

- spherical vortex ring—Hill [19] describes a steady state solution that assumes steady flow (inviscid) and uniform distribution of vorticity inside a sphere (vortex atmosphere) of radius a.

- thick vortex ring—such solutions are identified by a larger core radius to ring radius ratio (Limit as a/R $\rightarrow \sqrt{2}$; see **Figure 1**). These ideal models (e.g. Norbury-Fraenkel [20] [21], Kaplanski-Rudi [22]) begin by assuming a certain distribution of vorticity (linear, Gaussian). By matching the values of the integrals of motion of the swept volume to the corresponding values of the vortex ring, analytical expressions can be obtained.

- thin vortex ring—in contrast to the above, the thin ring approximation is characterised by a smaller core radius to ring radius ratio (Limit as a/R $\rightarrow$ 0) (Lamb [23]). This assumes constant vorticity inside the vortex core, enabling an analytical expression for the stream function inside the ring cross-section to be obtained.

Key characteristics are expressed analytically in **Table 1**. According to Saffman [24] ring core radius (a) is a function of the impulse (characterised by a temporal parameter *T*) used to generate the ring;
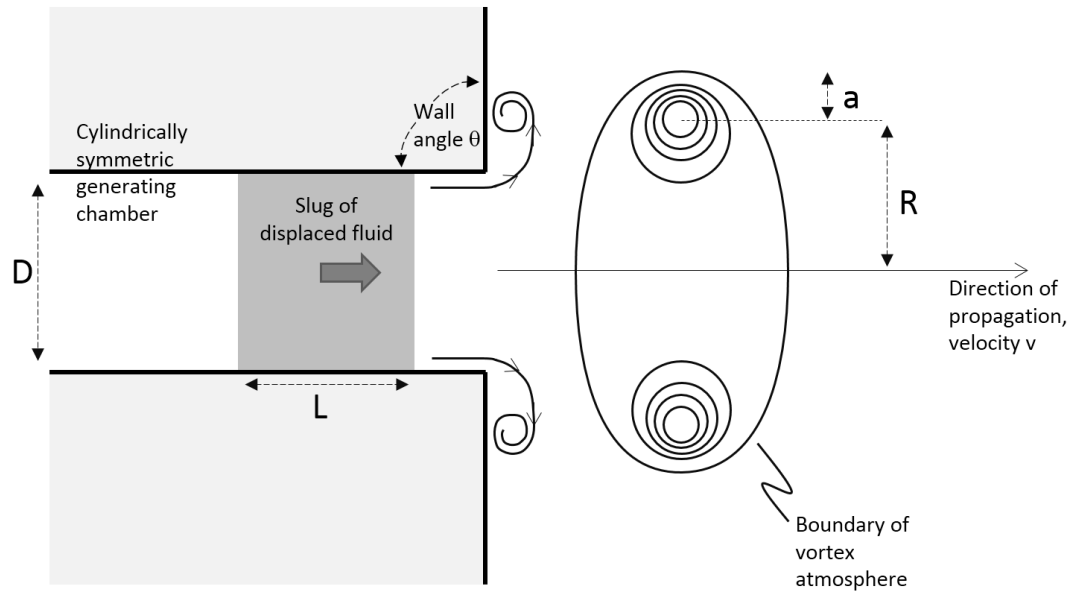
$$a = \sqrt{4vT} \tag{1}$$

Figure 1. Typical features of ring vortex generation. A slug of fluid is propelled through an orifice (stroke length *L*, stroke time *T*) and the fluid "rolls up" to create a torus of vorticity that detaches from the wall and propagates as a ring vortex with velocity *v*. The ring radius R is derived from the radial coordinate of the vortex center, identified with the maximum in the distribution of vorticity (approximately Gaussian). The core radius a is derived from the distribution of vorticity, defining the core as the region where the norma-lized vorticity $\bar{\omega} = \dfrac{\omega}{\omega_{max}} \geq 0.05$ [25].

and ring radius (R) is related to the impulsive volume of fluid used to generate the vortex (characterised by a length parameter *L*)[2]:

$$R = \left(\frac{3R_0^2 L}{4} \right)^{\frac{1}{3}} \tag{2}$$

These are important relationships that offer insights to ring vortex behaviour, with implications for physical phantom design.

2.2. Experimental

The analytical descriptions presented do not include any concept of ring vortex creation—the mathematics describes only the fluid dynamics once the ring has been generated. Experimental studies require a mechanism to create the vortex and this involves propelling a slug of fluid through an orifice. **Figure 1** illustrates this process. The ejected fluid is compelled to swirl around the orifice geometry to create a torus of vorticity that subsequently detaches from the wall and prop-agates through the free field. The geometry of the generator is cylindrically symmetric, although the wall angle θ does not need to be 90 degrees (the expe-rimental results presented in this paper use a wall angle of 45 degrees). In this study (**Figure 2**) a single one-half cycle of a low frequency sinusoidal oscillation (10 Hz) was coupled by way of an audio amplifier [Adafruit 20 W Stereo Audio

---

[2]The presented formula applies to the non-spherical vortex. The radius according to the Hill model is $R = a/\sqrt{2}$.
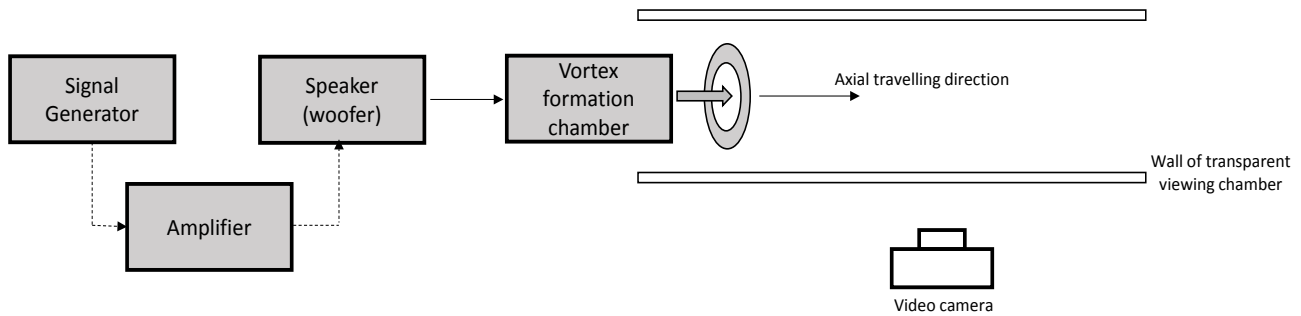
Figure 2. Schematic of the experimental system used in this study. A loud speaker (woofer) provided the mechanism for fluid slug ejection through a vortex formation chamber created with a 3D printer. A signal generator controlled displacement of the speaker using an audio amplifier. Smoke ring visualisation used a commercially available fluid consisting of a water/glycerol mixture vaporized with a mini smoke/fog machine. The ring propagated along a path enclosed by a large transparent tunnel—an attempt to minimise atmospheric disturbances.

Amplifier MAX9744 (USA)] to the displacing membrane of a loud speaker [Monacor SP-45/8 (Germany)] to propel a slug of fluid through an orifice with subsequent ring vortex creation and propagation.

For proof of concept purposes the experiment was performed in air, with the smoke filled generator chamber producing a visible smoke ring that was captured by video camera at 30 frames per second. With an orifice diameter of 1 centimetre, rings were generated at Reynolds numbers of 500, 1000 and 2000 in the orifice throat. Post processing of the digital video stream enabled salient features of the ring to be measured. Ring size and velocity were used to create plots of vortex behaviour as a function of time and distance.

2.3. Computational

The experimental system detailed above was simulated using a computational description. ANSYS Fluent [ANSYS Fluent 16.1 (Canonsburg, PA, USA)] was used to investigate the behaviour of the vortex ring, avoiding the idealisation constraints associated with the analytical formulation (see Figure 3).

The geometry modelled was a 2D axisymmetric domain from the vortex generator extending 50 cm in the direction of propagation of the vortex and 10 cm from the symmetry axis in the radial direction to represent the free field region. These axial and radial extents of the computational domain were chosen to be large enough to observe the propagation of the vortex ring over an extended distance (*i.e.* protracted time period) and to prevent the lateral and downstream pressure boundary conditions from affecting the dynamics of the propagating ring. A structured, mapped mesh of quadrilateral elements was employed, biased in the radial direction to obtain a high density of elements close to the symmetry axis, where the greatest velocity gradients would be located. Preliminary sensitivity tests were performed to determine appropriate mesh and time step size to provide acceptable numerical accuracy. Optimal values were 6.25×10^{-4} m for the mean size of the mesh elements and 1×10^{-3} s for the time step size. Residuals of 0.1% offered a satisfactory threshold for effective computation.

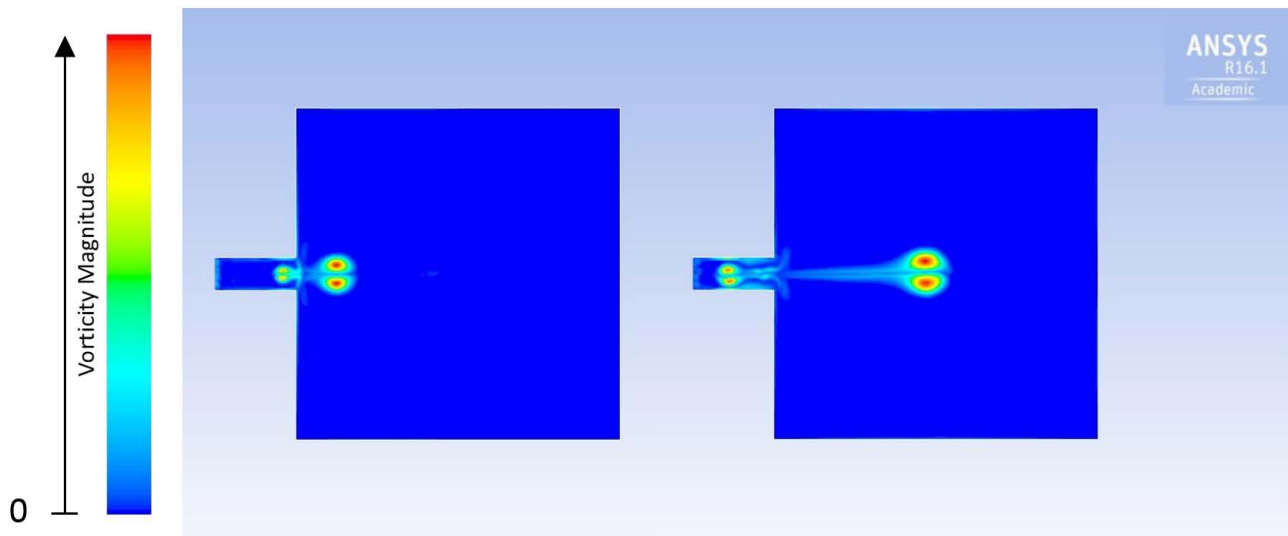Boundary conditions included simulation of the ring vortex generator speaker

Figure 3. Example CFD solutions (2D, axisymmetric) demonstrating generation and propagation of a ring vortex at Re = 2000. A slug of fluid expelled from the narrow channel at the left of the domain proceeds as a vortex ring that propagates to the right. The images plot vorticity, illustrating complex but stable and predictable flow features.

membrane, with the aim of reproducing the experimental conditions of the speaker displacement. The time dependent uniform inlet velocity (normal to the boundary) was of the form

$$U = U_0 \cos(wt) \quad \text{for} \quad t \leq T^*/4 \tag{3}$$

$$U = 0 (\text{zero velocity}) \quad \text{for} \quad t > T^*/4 \tag{4}$$

where t represents time and w refers to the angular frequency of membrane oscillation with period T^*. A no-slip condition was imposed on the internal and external surface of the vortex generator cavity, and zero gauge-pressure was present on all the other boundaries (free field). The initial condition for the velocity vector field was zero everywhere in the domain. Time to compute flows over a subsequent 1 second period on a 3.5 GHz PC (6 cores) was 4 hours.

3. Results

Figure 4 compares results obtained using the experimental and computational approaches to assess the dynamics of vortex motion within the domain. Experimental results are shown in Figure 4(a), Figure 4(c), Figure 4(e), Figure 4(g) and computational results are shown in Figure 4(b), Figure 4(d), Figure 4(f), Figure 4(h). Figure 4(a) and Figure 4(b) report the position of the ring as a function of time, the ring size (2R + 2a) versus time is shown in Figure 4(c) and Figure 4(d) with the change in ring velocity over time shown in Figure 4(e) and Figure 4(f). The curves derived from CFD data in Figure 4(d) and Figure 4(f) are not smooth as a result of spatial discretization. Finer meshes produce smoother curves at the cost of increased computing time.

The analytical solutions suggest simple relationships between ring size, velocity, time and position as follows;

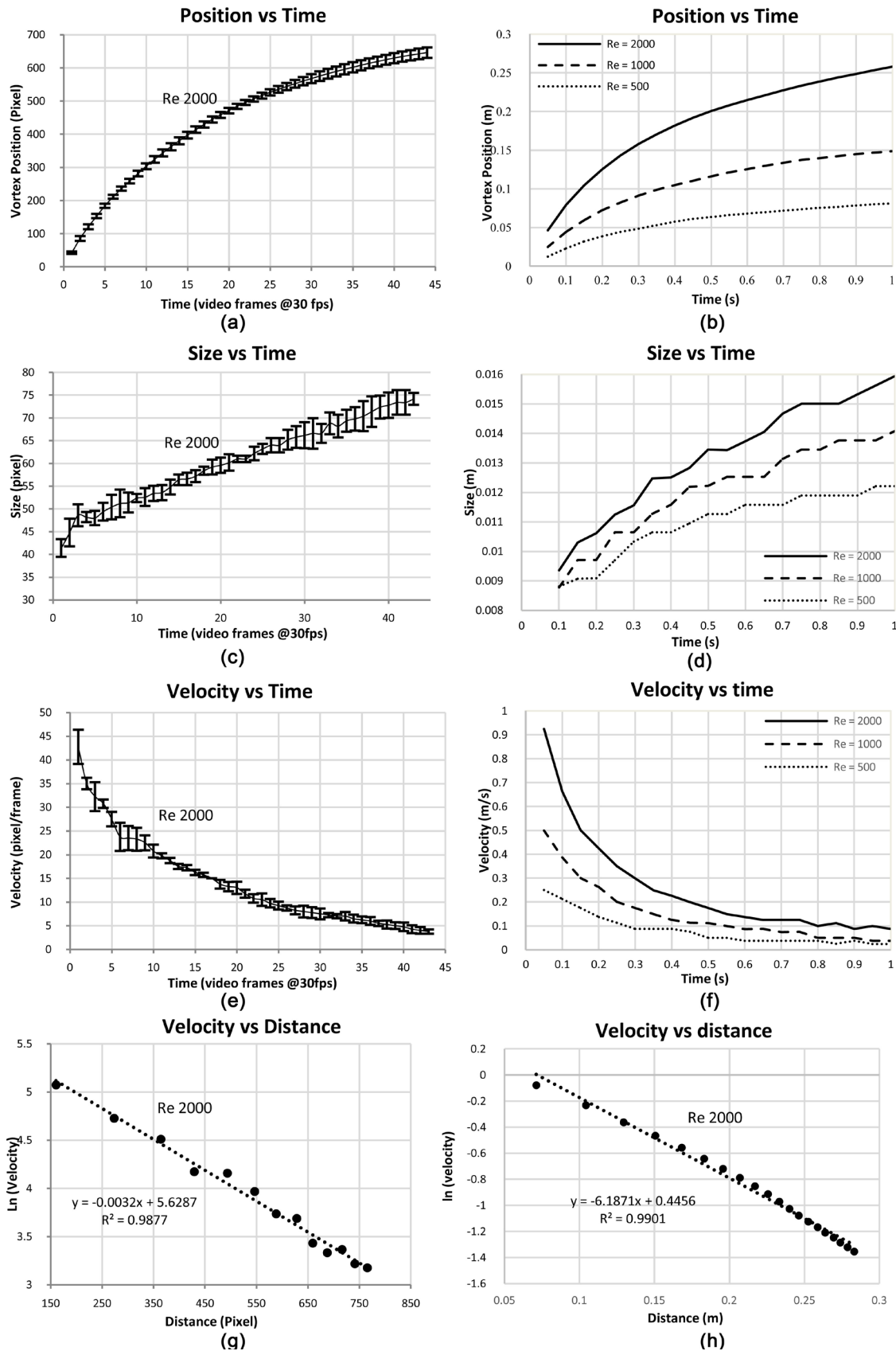- ring velocity varies with the reciprocal of time

Figure 4. Experimental and computational results relating to ring vortex position, size, and velocity. The graphs on the left hand of the page present experimentally measured data. The graphs on the right show directly comparable data obtained by numerical simulation.

- ring velocity varies exponentially with distance
- ring size can be expected to grow linearly with propagation time

Figure 4(g) and Figure 4(h) illustrate expected linear behaviour (log(velocity) plot), whereas Figure 5 presents the results of multiple experimental tests to clarify reproducibility of the ring vortex propagation. All experimental data was captured under the same experimental conditions. These plots show good agreement with the theoretical predictions and the reproducibility is encouraging. Repeated experimental trials typically produced identical ring behaviour to within 10%.
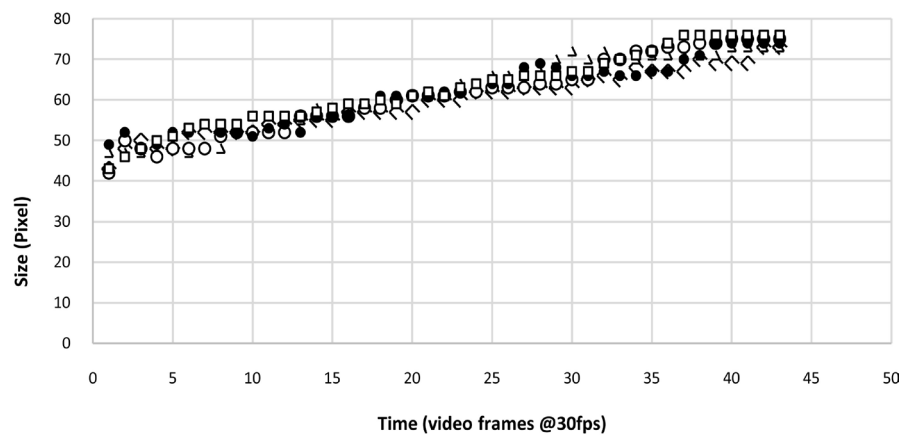
Ring Vortex Velocity - Reproducibilty
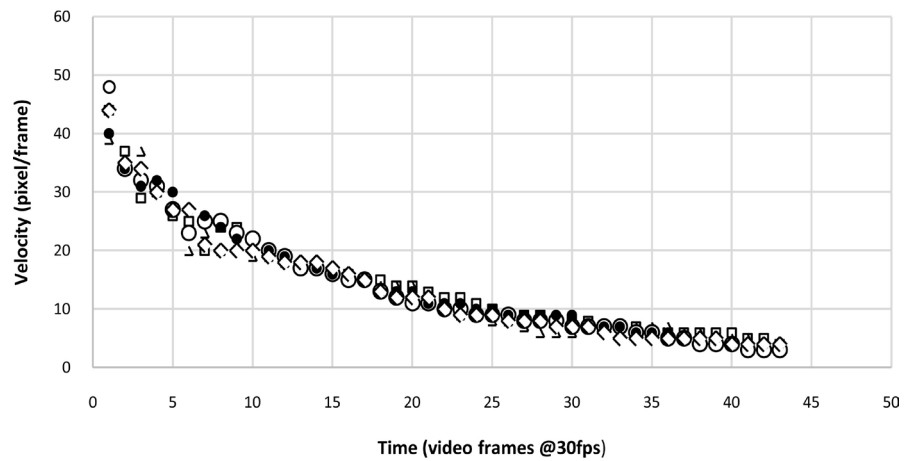
Experimental Results - Vortex Velocity - Reproducibility of 5 vortex rings from the experimental dataset, captured at 30 frames per second (fps)

(a)

Ring Vortex Size - Reproducibility

Experimental Results - Vortex Size - Reproducibility of 5 vortex rings from the experimental dataset, captured at 30 frames per second (fps)

(b)

Figure 5. Results illustrating reproducibility of ring vortex behaviour with multiple repeated experiments. Each vortex is represented by a different marker shape: ring 1 - o; ring 2 -•; ring 3 -◊; ring 4 -Δ; ring 5 -□. **Figure 5(a)** and **Figure 5(b)** plot ring velocity and ring size.

4. Discussion

4.1. Agreement between Experimental and Computational Behavior

The results reported in this study encourage use of the ring vortex as a complex flow benchmark for imaging. Notably the analytical, experimental and computational analyses of ring vortex behaviour are all in agreement. Key features of the flow which are well reproduced include:

- Ring diameter (2R) is dependent on swept volume of the piston (*i.e.* volume of the slug of displaced fluid)
- Ring core diameter (2a) is dependent on the velocity/energy of the slug of displaced fluid
- Ring velocity is dependent on slug velocity
- Ring velocity decays approximately exponentially with distance ($R^2 \approx 0.99$)

The numerical simulations are particularly helpful in confirming that most of the fluid volume displaced by the piston ($\pi D^2 L/4$) is transported into the ring annulus ($\approx 2\pi R \cdot \pi a^2$). A small proportion remains close to the central axis of the orifice channel (*i.e.* it remains separate from the core) and, by virtue of inertia, this proportion increases at higher Reynolds numbers (*i.e.* higher slug velocities). Consequently for a given volume of displaced fluid the core radius decreases for higher displacement velocities. Ring size (R) grows steadily with piston displacement (*L*) and the kinetic energy of the displaced fluid is largely converted into angular momentum to create the vorticity of the ring core. It is this that draws the ring through the fluid as it detaches from the wall. Consequently, the velocity of the piston determines the velocity of the ring. It was Reynolds [26] who first observed that, contrary to Kelvin's inviscid description [27], the volume of the vortex ring atmosphere continually increases due to entrainment of external fluid and its velocity decreases because its momentum has to be shared with a greater mass of fluid. Laminar shear combined with viscous losses is also an important mechanism for dissipation—energy is lost from the ring, vorticity is reduced, the ring slows and eventually breaks up. A trailing wake along the central axis of the ring is another feature of its propagation. This becomes increasingly evident and disturbed at high (Reynolds) ring velocities and is a symptom of ring instability, losses and break up.

Experimental results have been presented for *Re* = 2000 because the fluid behaviour in this regime (transitional within the throat of the orifice) can be expected to demonstrate greater instabilities/complexities than at *Re* = 1000 or *Re* = 500. Results at *Re* = 2000 tend to improve at lower Reynolds number, also confirmed by the CFD data shown in **Figure 4(b)**, **Figure 4(d)**, and **Figure 4(f)**. Furthermore, *Re* = 2000 is consistent with blood flow in human vessels in the presence of pathologies like stenosis [28]. It is also the Reynolds number suggested by the standard EN 61685-IEC 61685:2001 for the design of a flow test object for Doppler Ultrasound [9].

4.2. CFD Model Assessment

As an additional assessment of the validity of our computational approach, an

investigation involving reproduction and comparison with the work of Danaila and Hélie [29] was undertaken. This work considers the influence of the stroke ratio (*i.e.* stroke length L) and orifice diameter (D), on the main characteristics (e.g. topology, dynamics) of laminar vortex rings. Assessment of fidelity included our own independent computation of translational speed and determination of core radius. The former was estimated by tracking the position of the vortex centre, according to the definition given by Helmholtz [30], whilst the latter was quantified according to the definition given by Saffman [31]. Our analyses agreed with Danaila and Hélie to within 1%.

4.3. Application in Medical Imaging Assessment and Simulation Behaviour

It is important to recognise that flow phantoms set the standards against which scanner performance is judged, which by implication influences the diagnostic thresholds that are used to manage the patient treatment pathway. Consequently, poorly calibrated imaging systems adversely impact patient management, although there are no accepted, general imaging, independent standards for complex flow.

The ring vortex represents a reference flow that is both well understood yet complex, with direct physiological significance (ring vortices are reported to be a feature of ventricular action and are also associated with valve function [32]). The work of Toger *et al.* [33] is a rare example in which a ring vortex was used to validate 4DMRI interpretation of a specific cardiac flow. More widely (and more importantly), the ring vortex offers a controlled selection of complex flow features that are fundamental to any disturbed physiological flow. In the context of a phantom, desirable properties are:

- Predictability (within specified tolerances, the flow can be known at every point in space and time)
- Reproducibility (the flow is repeatable, it does the same thing every time)
- Controllability (the flow characteristics can be varied in a controlled fashion)
- Stability (the flow is robust and easy to produce; resistant to disturbances)

Critique of the vortex analyses presented here identifies that the analytical solutions are highly idealised, with assumptions that limit the relevance of their solutions to real world problems (e.g. phantoms). Nonetheless they do offer insight into ring vortex behaviour and are invaluable as a validation tool for numerical analyses (CFD). When the CFD is applied to real experimental geometries, it becomes a predictive tool suited to phantom design and its subsequent operation. Of course the assumptions associated with CFD modelling may not translate to effective description of actual ring vortex behaviour, but our experiments show otherwise—despite the proof of concept nature of these experiments undertaken in air—indicating correlation between theory and experimental behaviours. The vortex in air was chosen since construction of an air based system was cheap and effective. However, this does not come without compromises—neutral buoyancy of the visible smoke was lacking; the propagating ring was sen-

sitive to air currents within its environment despite being enclosed by a tunnel; smoke ring visibility was limited etc. Nonetheless encouraging controllability, predictability, reproducibility and stability of this complex flow was obtained, and there is good reason to anticipate much improved performance in a better controlled and more refined liquid environment. This opens numerous opportunities for flow phantom development, including the potential for a liquid-based programmable unit capable of delivering repeatable, precomputed complex flows to MRI, ultrasound and CT. A test object such as this could be used to generate cyclic flow features, produce accelerating behaviour consistent with pulsatility, or to deliver precise repeatable eddy formations by virtue of vorticity. All of this can be achieved in a reproducible manner consistent with previously established characterisation (from both theory and experiment). An aspirational goal would be the creation of a system that would present full field, dynamic and complex known flows at known tolerances to aid diagnostic interpretation of flow imaging data from existing medical imaging systems and to support novel imaging hardware and software design.

In the wider context of CFD benchmarking, the flexibility of such a flow phantom also has the potential to exercise and quantify the predictive capabilities (to within defined tolerances) of existing and novel computational approaches, particularly for flows at higher Reynolds numbers where laminar approximations may be insufficient to successfully capture flow behaviour.

5. Conclusion

This paper has reported analytical, experimental and computational behaviour of the ring vortex. The work demonstrates that this inherently complex flow has features that are sufficiently predictable, reproducible, controllable and stable to warrant its consideration as a candidate for a complex flow phantom in medical imaging. A flow benchmark such as this also has implications for quality assurance of numerical simulation methodologies.

Acknowledgements

References

[1] Schnell, S., Wu, C. and Ansari, S.A. (2016) Four-Dimensional MRI Flow Examinations in Cerebral and Extracerebral Vessels—Ready for Clinical Routine? *Current Opinion in Neurology*, **29**, 419-428.
https://doi.org/10.1097/WCO.0000000000000341

[2] Hecht, H.S., Narula, J. and Fearon, W.F. (2016) Fractional Flow Reserve and Coronary Computed Tomographic Angiography: A Review and Critical Analysis. *Circulation Research*, **119**, 300-316. https://doi.org/10.1161/CIRCRESAHA.116.307914

[3] Whitlock, M.C. and Hundley, W.G. (2015) Noninvasive Imaging of Flow and Vascular Function in Disease of the Aorta. *JACC Cardiovascular Imaging*, **8**, 1094-

1106. https://doi.org/10.1016/j.jcmg.2015.08.001

[4] Mongeon, F.P., Marcotte, F. and Terrone, D.G. (2016) Multimodality Noninvasive Imaging of Thoracic Aortic Aneurysms: Time to Standardize? *Canadian Journal of Cardiology*, **32**, 48-59. https://doi.org/10.1016/j.cjca.2015.09.025

[5] Adam, A., Dixon, A.K., Gillard, J.H., Schaefer-Prokop, C., Grainger, R.D. and Allison, D.J. (2014) Grainger & Allison's Diagnostic Radiology. 6th Edition, Churchill Livingstone Elsevier, London.

[6] Kilner, P.J., Gatehouse, P.D. and Firmin, D.N. (2007) Flow Measurement by Magnetic Resonance: A Unique Asset Worth Optimising. *Journal of Cardiovascular Magnetic Resonance*, **9**, 723-728. https://doi.org/10.1080/10976640701465090

[7] Hariharan, P., Giarra, M., Reddy, V., Dat, S.W., Manning, K.B., Deutsch, S., Stewart S.F.C., Myers, M.R., Berman, M.R., Burgreen, G.W., Paterson, E.G. and Malinauskas, R.A. (2011) Multilaboratory Particle Image Velocimetry Analysis of the FDA Benchmark Nozzle Model to Support Validation of Computational Fluid Dynamics Simulations. *Journal of Biomechanical Engineering*, **133**, Article ID: 041002.

[8] ISO 9001:2015—Requirements of a Quality Management System; ISO 9000:2015—Concepts and Language; ISO 9004:2009—Making a Quality Management System More Efficient and Effective; ISO 19011:2011—Guidance on Internal and External Audits of Quality Management Systems.
http://www.iso.org/iso/home/standards.htm

[9] BS EN 61685:2002, IEC 61685:2001. Ultrasonics. Flow Measurement Systems. Flow Test Object, 14th February 2002.

[10] Browne, J.E. (2014) A Review of Doppler Ultrasound Quality Assurance Protocols and Test Devices. *Physica Medica*, **30**, 742-751.
https://doi.org/10.1016/j.ejmp.2014.08.003

[11] Lai, S.S., Yiu, B.Y., Poon, A.K. and Yu, A.C. (2013) Design of Anthropomorphic Flow Phantoms Based on Rapid Prototyping of Compliant Vessel Geometries. *Ultrasound in Medicine & Biology*, **39**, 1654-1664.
https://doi.org/10.1016/j.ultrasmedbio.2013.03.015

[12] Chee, A.J., Ho, C.K., Yiu, B.Y. and Yu, A.C. (2016) Walled Carotid Bifurcation Phantoms for Imaging Investigations of Vessel Wall Motion and Blood Flow Dynamics. *IEEE Transactions on Ultrasonics, Ferroelectrics, and Frequency Control*, **2016**, 1852-1864. https://doi.org/10.1109/TUFFC.2016.2591946

[13] Grice, J.V., Pickens, D.R. and Price, R.R. (2016) Technical Note: A New Phantom Design for Routine Testing of Doppler Ultrasound. *Medical Physics*, **43**, 4431.
https://doi.org/10.1118/1.4954205

[14] Hoskins, P.R. (2008) Simulation and Validation of Arterial Ultrasound Imaging and Blood Flow. *Ultrasound in Medicine & Biology*, **34**, 693-717.
https://doi.org/10.1016/j.ultrasmedbio.2007.10.017

[15] Kweon, J., Yang, D.H., Kim, G.B., Kim, N., Paek, M., Stalder, A.F., Greiser, A. and Kim. Y.H. (2016) Four-Dimensional Flow MRI for Evaluation of Post-Stenotic Turbulent Flow in a Phantom: Comparison with Flow Meter and Computational Fluid Dynamics. *European Radiology*, **26**, 3588-3597.

[16] Akhmetov, D.G. (2009) Vortex Rings. Springer-Verlag, Berlin Heidelberg.

[17] White, F.M. (1999) Fluid Mechanics. McGraw-Hill, Boston.

[18] Tryggeson, H. (2007) Analytical Vortex Solutions to the Navier-Stokes Equation. Thesis for the Degree of Doctor of Philosophy, Växjö University, Växjö.

[19] Hill, M.J.M. (1894) On a Spherical Vortex. *Proceedings of the Royal Society of London*, **55**, 219-224. https://doi.org/10.1098/rspl.1894.0032

[20] Norbury, J. (1973) A Family of Steady Vortex Rings. *Journal of Fluid Mechanics*, **57**, 417-431. https://doi.org/10.1017/S0022112073001266

[21] Fraenkel, L.E. (1972) Examples of Steady Vortex Rings of Small Cross-Section in an Ideal Fluid. *Journal of Fluid Mechanics*, **51**, 119-135. https://doi.org/10.1017/S0022112072001107

[22] Kaplanski, F. and Rudi, U. (1999) Dynamics of a Viscous Vortex Ring. *International Journal of Fluid Mechanics Research*, **26**, 5-6. https://doi.org/10.1615/interjfluidmechres.v26.i5-6.60

[23] Lamb, H. (1932) Hydrodynamics. Cambridge University Press, Cambridge.

[24] Saffman, P.J. (1992) Vortex Dynamics. Cambridge University Press, Cambridge.

[25] Zhao, W., Steven, H.F. and Mongeau, L.G. (2000) Effects of Trailing Jet Instability on Vortex Ring Formation. *Physics of Fluids*, **12**, 589. https://doi.org/10.1063/1.870264

[26] Reynolds, O. (1876) On the Resistance Encountered by Vortex Rings and the Relation between Vortex Rings and the Stream-Lines of a Disc. *Nature*, **14**, 477-479.

[27] Kelvin, W.T.B. (1878) Vortex Statics. *Proceedings of the Royal Society of Edinburgh*, **9**, 59-73. https://doi.org/10.1017/S0370164600031679

[28] Bale-Glickman, J., Selby, K., Saloner, D. and Savas, O. (2003) Experimental Flow Studies in Exact-Replica Phantoms of Atherosclerotic Carotid Bifurcations under Steady Input Conditions. *Journal of Biomechanical Engineering*, **125**, 38-48. https://doi.org/10.1115/1.1537734

[29] Danaila, I. and Hélie, J. (2008) Numerical Simulation of the Post Formation Evolution of a Laminar Vortex Ring. *Physics of Fluids*, **20**, Article ID: 073602.

[30] Helmholtz, H. (1858) Über Integrale der hydrodynamischen Gleichungen, welche den Wirbelbewegungen Entsprechen. *Journal für die reine und angewandte Mathematik*, **55**, 25-55. https://doi.org/10.1515/crll.1858.55.25

[31] Saffman, P.G. (1978) The Number of Waves on Unstable Vortex Rings. *Journal of Fluid Mechanics*, **84**, 625-639. https://doi.org/10.1017/S0022112078000385

[32] Vedula, V., George, R., Younes, L. and Mittal, R. (2015) Hemodynamics in the Left Atrium and Its Effect on Ventricular Flow Patterns. *Journal of Biomechanical Engineering*, **137**, Article ID: 111003. https://doi.org/10.1115/1.4031487

[33] Toger, J., Kanski, M., Carlsson, M., Kovacs, S.J., Soderlind, G., Arheden, H. and Heiberg, E. (2012) Vortex Ring Formation in the Left Ventricle of the Heart: Analysis by 4D Flow MRI and Lagrangian Coherent Structures. *Annals of Biomedical Engineering*, **40**, 2652-2662. https://doi.org/10.1007/s10439-012-0615-3